7th International Conference on Water Resources and Arid Environments (ICWRAE 7): 242-257
4-6 December 2016, Riyadh, Saudi Arabia

Groundwater Potentiality at El Egma Plateau, Central Sinai, Egypt Using Geoelectrical, Gravity and Magnetic Data

[1]Sultan Awad Sultan Araffa, [2]Hassan S. Sabet and [3]Mahmoud S. Shehata

[1]National Research Institute of Astronomy and Geophysics (NRIAG, Egypt)
[2]Geology Dep. Faculty of Science, Al-Azhar University, Cairo, Egypt
[3]Ceramica Cleopatra Group Company, Suez, Egypt

Abstract: In the present study different geophysical techniques such as Vertical Electrical Sounding, Gravity and Magnetic are used to delineate the deep aquifer in the South El-Egma area. The area under study is located in the central part of Sinai Peninsula, Egypt. In this area eighteen deep vertical electrical soundings have been carried out, using current electrode spacing (AB) ranging from 10 m to 6000 m to reach the deep aquifer in the study area. The results of resistivity interpretation indicate that; the study area consists of five geoelectric units. The fifth geoelectric unit represents the main groundwater aquifer in the study area (Nubian Sandstone). The depth of the upper surface of the Nubian sandstone aquifer was ranging from 718 m to 927 m, resistivity varies between 26.5 Ohm.m and 477 Ohm.m and the thickness ranges from 191 m to 3330 m. Five hundred and twenty-one gravity stations have been collected by using CG-3 Gravity-meter. The results of quantitative interpretation for gravity data revealed that, the area was dissected by different normal fault elements of trends NE-SW and N-S. Four hundred and eighty-seven magnetic measurements were done to detect the basement depth and then the thickness of sedimentary deposits. The results of magnetic method reflected that, the depth of basement was ranging from 1005 m to 4108 m. The present study aims to exploration the groundwater and assessment of the Nubian sandstone aquifer in Central Sinai, Egypt by using geoelectrical, gravity and magnetic data, where the people who live in central Sinai suffer from scarcity of water for domestic and agricultural purpose

Key words: Groundwater Evaluation · Geophysical Interpretation · South El-Egma Plateau · Central Sinai · Egypt

INTRODUCTION

The interpretation of integrated geophysical data is becoming standard in applied geophysics, especially geoelectrical, electromagnetic, magnetic, gravity and, more recently, nuclear magnetic resonance methods that are commonly used in groundwater exploration [1].The geoelectrical tools have been widely used to delineate the shallow subsurface stratigraphy, groundwater sources and their quality [2].The gravity and magnetic methods are also used in groundwater exploration for delineating the subsurface structural elements and their trends, which are controlling the geometry of the groundwater aquifers [3].

The main target of the present study is to evaluate the groundwater occurrences to estimate the parameters of the deep groundwater aquifer (Nubian Sandstone aquifer) through the geophysical investigation and also to map the geologic subsurface structures and to detect the basement relief of the study area which located at the central part of Sinai, Egypt.

Location: The study area lies at the central part of Sinai Peninsula at longitudes 33° 10` and 34° 10` E and between latitudes 29° 30` and 30° 00` N and occupies an area of 5308 Km² (Fig.1). The study area is located in the area between the Gulf of Suez and Gulf of Aqaba and occupies low lands which can be used for different activities such as agricultural and industrial projects.

Geology of the Area: The general geology of the study area is presented based on the geologic map which constructed by [4]. The most parts of the study area are covered by Holocene which composed of Wadi and

Corresponding Author: Sultan Awad Sultan Araffa, National Research Institute of Astronomy and Geophysics (NRIAG, Egypt)

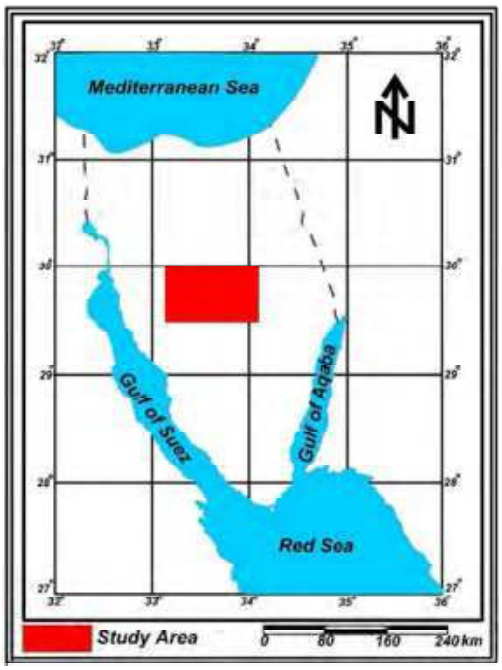

Fig.1: Location of the study area

Table 1: Geological description of borehole Jica1

TDS 1,206 Latitude 2 9°42'31" S.W.L 312.8m(BGL)			Elevation 520 longtude33°39r 08" Depthlt254 m
Water Bearing Formation: Nubian			Sandstone (Lower cretaceous).
Depth (in)			

From	To	Age	Description
0	50	Paleocene	Wadi Deposits
50	ISO	Maastrichtian	Limestone intercalated with clay
ISO	270	Campanian	Claystone
270	585	Santonian-Coniacian	Limestone intercalated with clay
585	450	Turonian	Limestone
450	520		Chalky Limestone
520	585	Cenomanian	Limestone intercalated with clay
585	640		Limestone
640	670		Limestone intercalated with clay
670	700		Limestone
700	770		Limestone intercalated with clay
770	810		Limestone
810	865		Limestone intercalated with clay
S65	1115	Lower Cretaceous	Alternation of shale and Sandstone
ms	1260	Jurassic	Sand and Shale

Pleistocene deposits, of alluvium deposits. These deposits overlay Paleocene deposits, including Esna Shale Formation which is composed of marly shale. Many stratigraphic units are ranging from the Upper Cretaceous to the Lower Eocene cover the eastern part of the area. The Lower Eocene deposits which are represented by Egma Formation of chalky limestone are located at the eastern and central parts of study area. The Upper Cretaceous is represented by Sudr Formation, which is composed of chalk of Maastrichtian age which is located at the western part; Duwai Formation is composed of alternating of carbonates and clastic of Campanian age at the western part of the study area; Matullah Formation is composed of limestone of Coniacian–Santonian age; and Wata Formation composed of dolomitic limestone of Coniacian–Turonian deposits. The subsurface stratigraphy of the study area is represented from the Jica well No.1 [5], which lies at the coordinate (Lat. 29°42′ 31″ and Long. 33°39′ 08″), with depth of 1254 m (Table 1). The stratigraphy of this borehole consists of Wadi deposits (Paleocene) which are composed of alluvial deposits of thickness of 59 m. Sudr Formation (Upper Senonian) is composed mainly of white chalk and chalky limestone of thickness 220 m. Matulla Formation of Lower Senonian is composed of white limestone intercalated with shale and marl, of thickness about 115 m. Wata Formation (Turonian), composed of two parts, the upper and middle parts consist of limestone with thickness 65 m. The lower part of Wata Formation consists of chalky limestone, with a thickness of 70 m which composed of limestone with minor breaks of shale. Cenomanian deposits are extended from 520 m to 861 m. Lower Cretaceous deposits are represented by Malha Formation or Nubian Sandstone facies that is non – fossiliferous thick section of fine to coarse grained sandstones intercalated with shale, limestone and marl units. The Lower Cretaceous rocks are represented in the Jica well No.1 at depth of 865 m. This formation is the main deep groundwater aquifer, especially in Sinai.

MATERIALS AND METHODS

Electrical Resistivity Data: Electrical resistivity techniques are well-established and widely used to solve a variety of geotechnical, geological and environmental problems ([6], [7], [8] and [9]). The electrical resistivity data used in this study include eighteen vertical electrical soundings (VES), were collected by using Schlumberger configuration of current electrode spacing (AB) ranging from 10 m to 6000 m. The main target of this tool is to detect the Nubian Sandstone aquifer in the study area (Fig.3). VES 9 was measured beside one borehole drilled in the study area (JICA1) for calibration the results of interpretation of geoelectrical data with the lithological units of the borehole (Fig.4). The electrical measurements were measured along the wadis (valleys) of directions north-south (N–S) and northeast-southwest (NE–SW) through the study area. The authors applied two techniques of quantitative interpretation to determine the true resistivity and thickness values of the successive strata of the subsurface section The first one is the manual interpretation, which depending upon the matching of the plotted field curves, on using two layers with the standard curves of the generalized Cagniard graphs ([10] and [11]). The obtained results of the manual interpretation have been used as initial models for the analytical methods by the second technique. The second technique was made using the IPI2WIN program. The quantitative interpretation has been applied to the data to determine the thicknesses and true resistivity's of the stratigraphic units, beside of each VES station as, final results (Fig.5).

Gravity Data and Analysis: Gravimetric field survey and measurements are carried out by the CG-3 Autograv (made by Scintrex, with reading resolution of 0.01 mGal). Five hundred and twenty-one gravity stations are collected at the available sites in the study area (Fig.6). All gravity measurements are corrected to different gravity corrections; such as, drift, tide, free-air, Bouguer, latitude and topographic corrections using specialized Geosoft software [12]. The terrain correction was also carried out using a Hammer chart and topographic maps of scale 1:50 000 to determine the mean elevations of the different zones for the hammer chart. Bouguer anomaly map was constructed from the corrected gravity data and used for qualitative and quantitative interpretation using [13] with a contour interval of 1 m Gal (Fig.7). The anomalies which observed in the Bouguer anomaly map are caused by lateral density variation within the sedimentary rocks, crust and sub-crust of the earth. The gravity anomaly map (Fig.7) shows that, the Bouguer anomaly field in the area ranges between a maximum value (-16.4 m.Gal) at the SE, SW, NW and West of the study area and a minimum value (-49.7 m.gal) at the northern, northeastern and southern of central part of the study area. The most significant features in the Bouguer gravity anomaly map are the steep gradients occur between high to low gravity values.

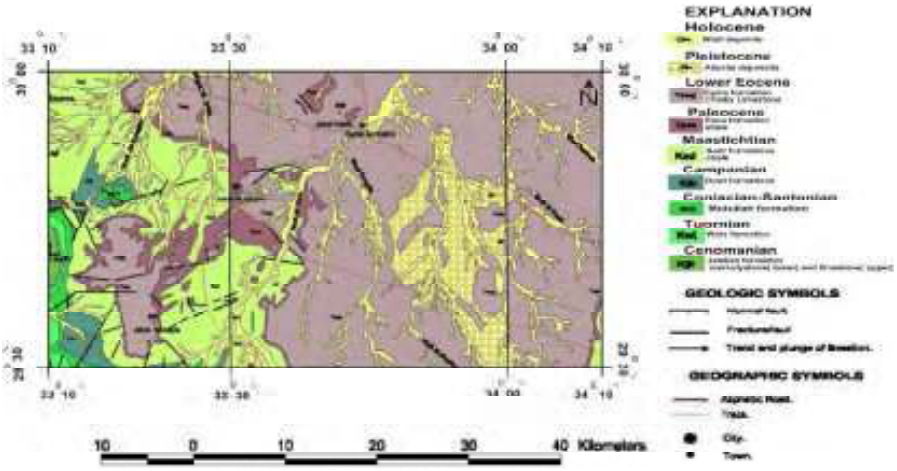

Fig. 2: Geologic map of the study area

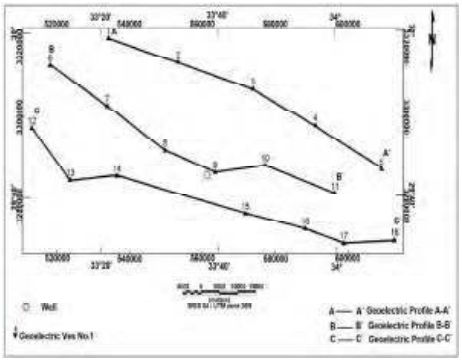

Fig. 3: Location map of Geoelectric Measurements

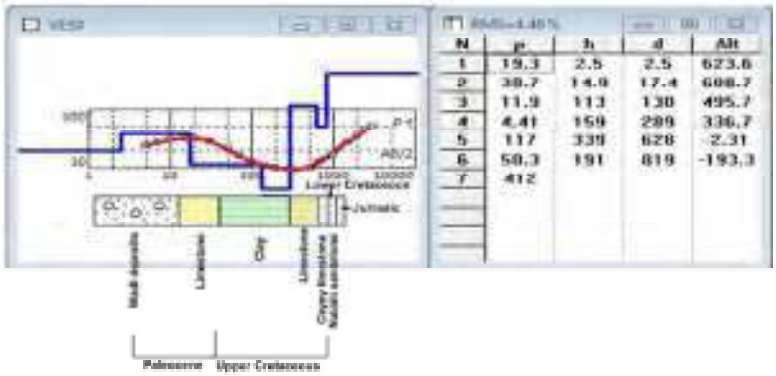

Fig. 4: Correlation between Jica1Well and VES No.9

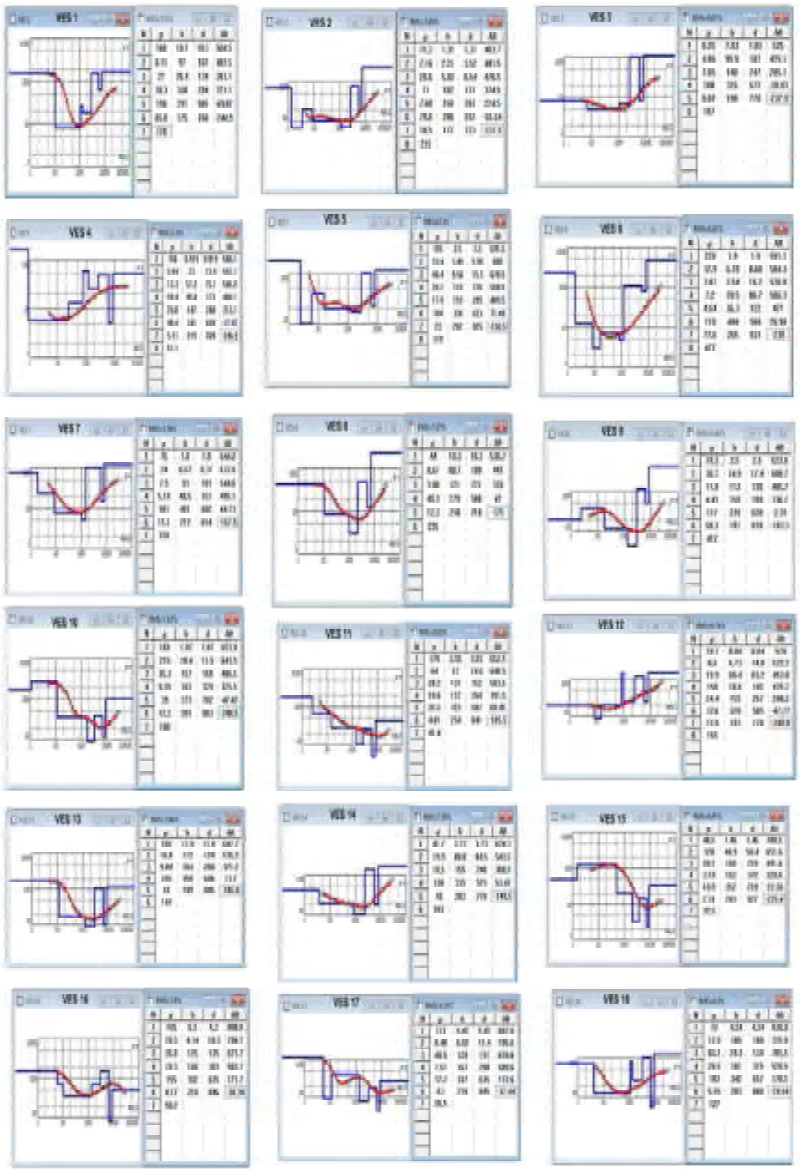

Fig. 5: 1-D VES interpretation Using IPI2WIN Program

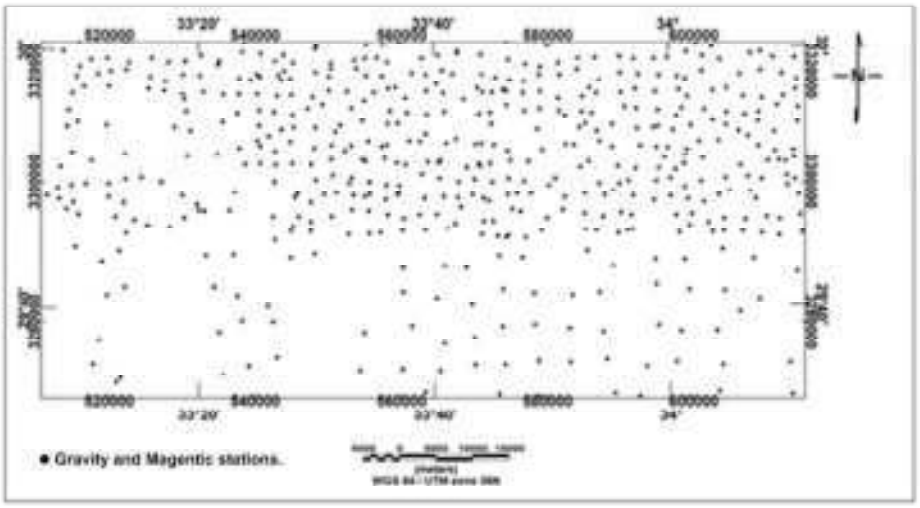

Fig. 6: Location map for Gravity and Magnetic stations

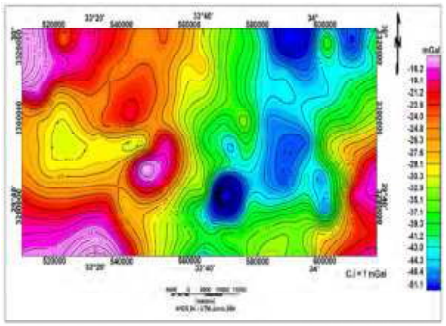

Fig. 7: Gravity Anomaly Map

Gravity Separation: The authors used least squares technique for gravity separation, this technique is a mathematical method applied on the gravity anomaly map to calculate the regional and residual maps. In the present study the least squares technique has been applied to separate the regional component (*Z*) from the Bouguer anomaly (*Δg*) (Abdelrahman *et al*, 1985). The residual component (*R*) can be estimated as follow:

$$R = \Delta g - Z \quad (1)$$

where:

$$\sum R^2 = Minimum \quad (2)$$

The regional surface is represented by a polynomial surface (Oldham and Sutherland 1955; Grant, 1957; and Van Voorhis and Davis, 1964), as known:

$$Z(x,y) = \sum_{n=0}^{p} \sum_{s=0}^{n} a_{n-s,s} x^{n-s} y^{s} \quad (3)$$

where:

$$a_{n-s,s} = \frac{1}{2}(p+1)(p+2) \quad (4)$$

$a_{n-s,s}$ is Coefficients.
p is the order of the two dimensional (2 D) polynomial.
x and y are the coordinates.
Z is the regional component.

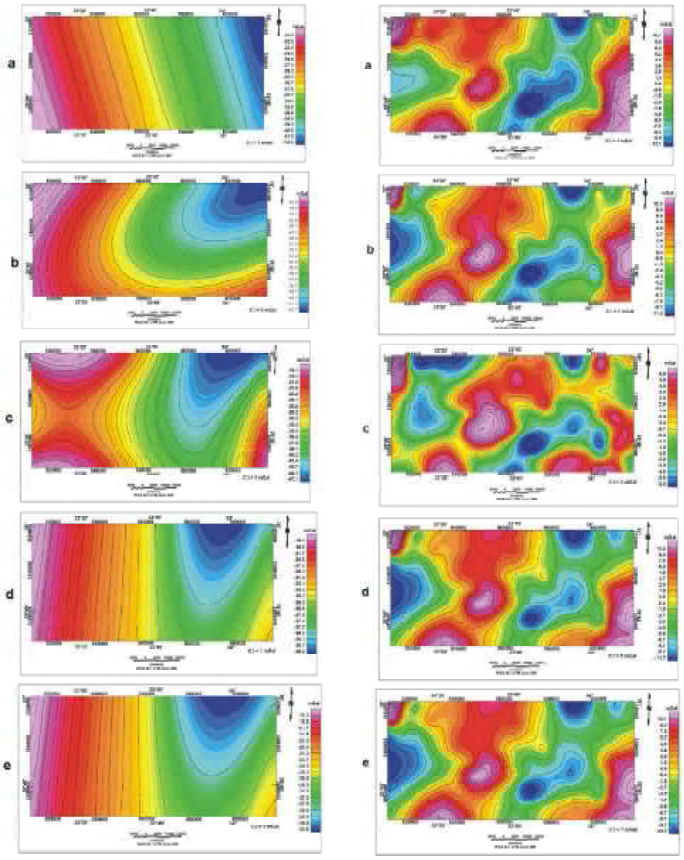

Fig. 8: Residual Gravity Anomaly Maps, a: First order, b: Second order, c: Third order, d:Fourth order, e:Fifth order

Fig. 9: Regional Gravity Anomaly Maps, a: First order, b: Second order, c: Third order, d:Fourth order, e:Fifth order

In the present work, the calculations were carried out to select the best order of residual for gravity separation. The best order was the fourth order. The residual component has been estimated by subtracting the regional values (Z) from the Bouguer values (Δg). The results of the separation of regional and residual for the different orders were mapped by (Oasis Montaj, 2007). The regional and residual components for the first to fifth orders are presented in Fig.8a-e and Fig.9a-e, respectively. A correlation factor $r(x,y)$ had been calculated to select the best order of residual for gravity interpretation. The correlation factor can be estimated for any two orders as follows:

$$r(x,y) = \frac{\sum xy - \frac{(\sum x)(\sum y)}{n}}{\sqrt{\left[\left(\sum x^2 - \frac{(\sum x^2)}{n_x}\right)\left(\sum y^2 - \frac{(\sum y^2)}{n_y}\right)\right]}} \quad (5)$$

The results are given in Table (2). The fourth order (r_{45}) is the best for gravity interpretation.

Table 2: Correlation Factors.

Correlation Factors	Value
r_{12}	0.8349
r_{23}	0.8646
r_{34}	0.81283
r_{45}	0.9998
r_{56}	0.9998

Magnetic Data and Analysis: The magnetic survey and measurements were carried out using two Envimag magnetometers (model Scintrex) made in Canada (1992) of 1 nT sensitivity. The measurements were collected at same sites of gravity measurements (Fig. 6) where the magnetic measurements had been measured using two magnetometers, the first one used for collecting data and the other one used for base station recordings, to apply the diurnal variations correction, to record the measurements automatically every one minute. Another correction (IGRF) was applied to remove the normal gradient of the magnetic field on the study area. The second instrument was used for the magnetic survey of the studied area. The calculation of the diurnal variation and IGRF were carried out by the [13]. The corrected magnetic data had been presented as a total intensity magnetic map, as shown in Fig 10. The total intensity magnetic map was reduced to the magnetic pole (RTP) to solve the dipole polarity and distortion of magnetic anomalies where it is a more interpretable map. This mathematical procedure was first described by [14], [15], [16] and [17]. The total intensity magnetic map after being reduced to the pole (Fig11.) indicates that, in comparison with the original total intensity magnetic map, reflected the northward shift in the positions of the inherited magnetic anomalies due to the elimination of the inclination of the magnetic field at this area. Also, the number of anomalies becomes larger, with comparable decrease of their aerial extension and the increase of their vertical reliefs. Added, the magnetic gradients become more intensive and steeper, giving rise to more resolution in both the encountered structural and lithologic inferences. By this way, the high and low magnetic anomalies formerly described in the total intensity magnetic map is well cleared in the total intensity magnetic map reduced to the pole with the appearance of some anomalies and the others are hidden. These could be seen in the southern part of the area, in which some

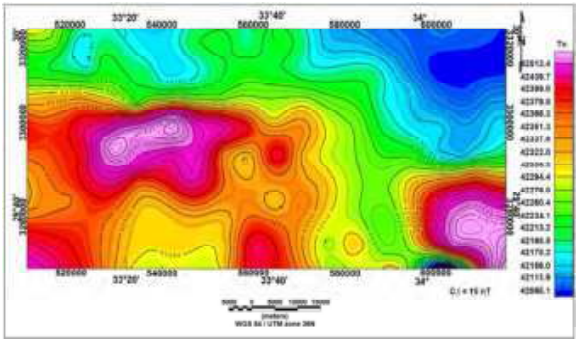

Fig. 10: Total Intensity Magnetic Map

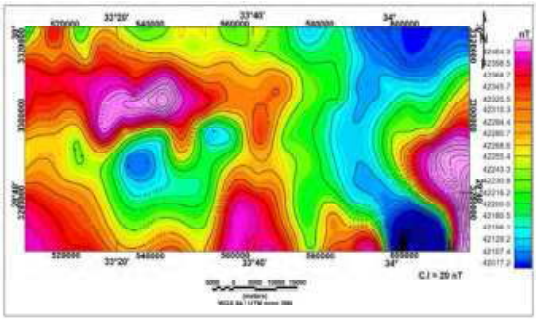

Fig. 11: Total Intensity Magnetic Map Reduced to the Pole (RTP Map).

anomalies appeared at the north of the central part with shifting for some anomalies to the north and the amplitudes of them were steeper than the total intensity magnetic map. Also, the appearance of some anomalies in the central part of the area, as well as at the southern part of the study area, some smaller positive and negative anomalies which present in the total intensity magnetic map, are concealed in the reduced magnetic pole map (and also some anomalies are disappeared from the RTP Map). Besides, the magnetic gradients in the total intensity magnetic map were shifted in their directions, most of them took the NNE-SSW and NNW-SSE trends. The principal application of the magnetic data is to determine the depth to the top of the geologic sources that produce observed anomalies. The magnetic tool was applied in the present study to determine the depth of basement rocks and then thickness of the sedimentary cover. 2D magnetic modeling was applied using GM-sys program, (Oasis Montaj, 2007) and then constructing a basement relief map from the results of 2D magnetic modeling.

RESULTS AND DISCUSSIONS

The results of the 1D-VES inversion of VES interpretation have been used for the construction of three geoelectrical cross sections. The three geoelectric cross-sections were constructed along three profiles (A-A`, B-B` and C-C`) oriented approximately NW–SE. The cross-sections are shown in Fig. 12 a, b and c, indicating that, the shallow subsurface lithologic sequence, in the study area, is represented by five geoelectric units. The first geoelectric unit is formed of chalky limestone of thickness ranging from 81 m at VES No.14 to 208 m at VES No.15 and its resistivity value ranged from 10 Ohm m at VES No.3 to 169 Ohm m at VES No.15. The second unit, corresponding to clays which were characterized by low resistivity values ranging from 2.5 Ohm m at VES No.5 to 70.3 Ohm m at VES No.16 with a thickness of 35 m at VES No.6 to 181 m at VES No.18. The third geoelectric unit, is associated with chalk and shaly limestone, showed relatively high resistivity values ranging from 14.9 Ohm m at VES No.15 to 158 Ohm m at VES No.1 and the thickness of this unit was ranging from 279 m at VES No.8 to 451 m at VES No.7 and its resistivity values ranged from 14.9 Ohm.m at VES No.15 to 158 Ohm m at VES No.1. The fourth geoelectric unit was formed from limestone intercalated with clay. The thickness of this unit was ranging from 118 m at VES No.3 to 265 m at VES No.6 and its resistivity values ranged from 2.3 Ohm m at VES No.15 to 77.6 Ohm m at VES No.6. The fifth unit was characterized by relatively moderate resistivity values ranging from 26.5 Ohm m at VES No.17 to 477 Ohm m at VES No.6 and correspond to sand and sandstone (Fig13a). According to the borehole results (Jica1), this unit contains the main (freshwater) groundwater aquifer in the area. The values of true resistivity for the Nubian sandstone were relatively high; indicating the quality of water was good due to the salinity was low. The total dissolved salts were 1206 ppm from the chemical analysis of the borehole Jica1. The depth of the fifth unit (Nubian Sandstone aquifer) was ranging from 718 m to 927 m (Fig13b).

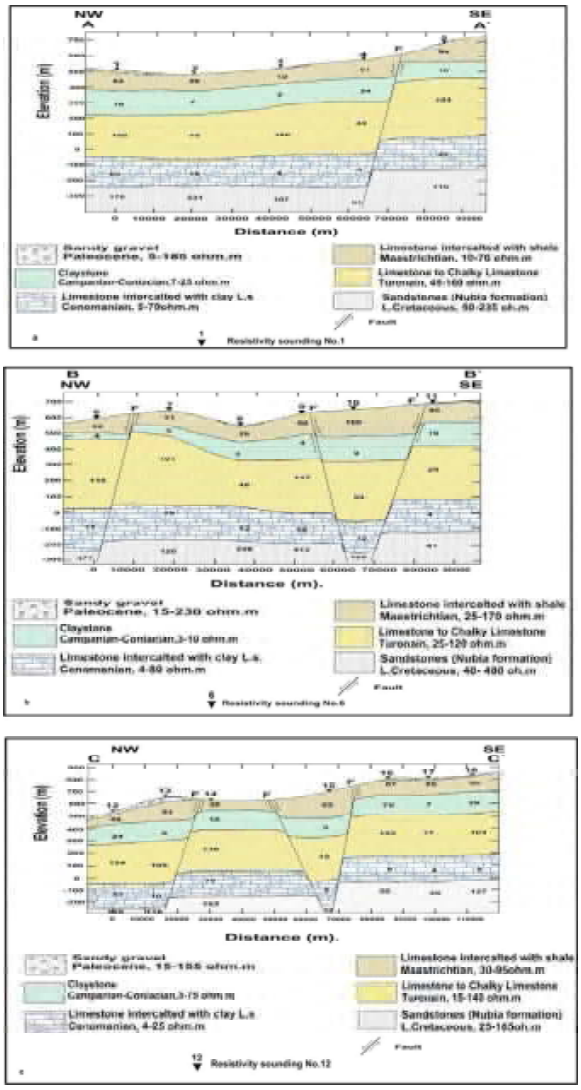

Fig. 12: Geoelectric Cross-Sections a, b and c long VES.1 to 18

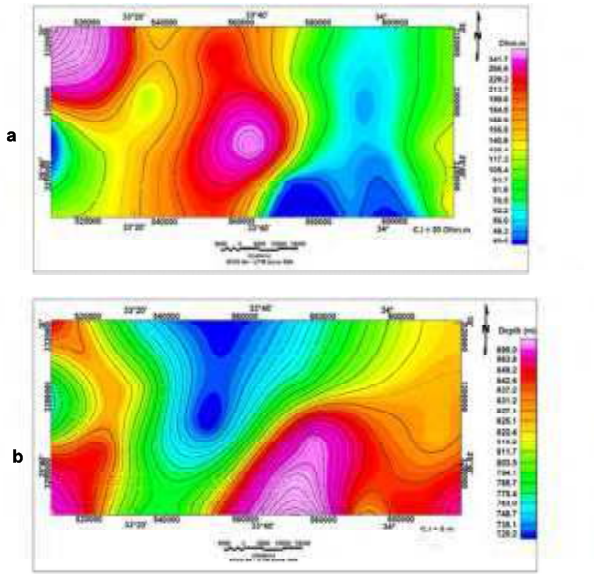

Fig.13: a: Isoresistivity, b: Depth map of the main aquifer (Nubian Sandstone)

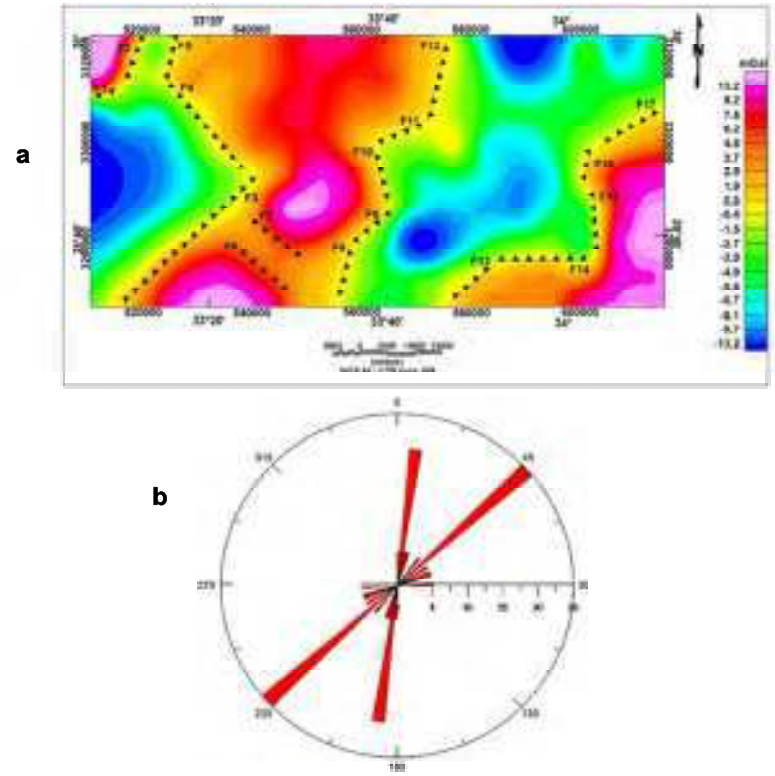

Fig. 14: a:Fault elements from Fourth order residual gravity anomaly map, b: Rose Diagram represents the trends of the structural elements which dissect the study area

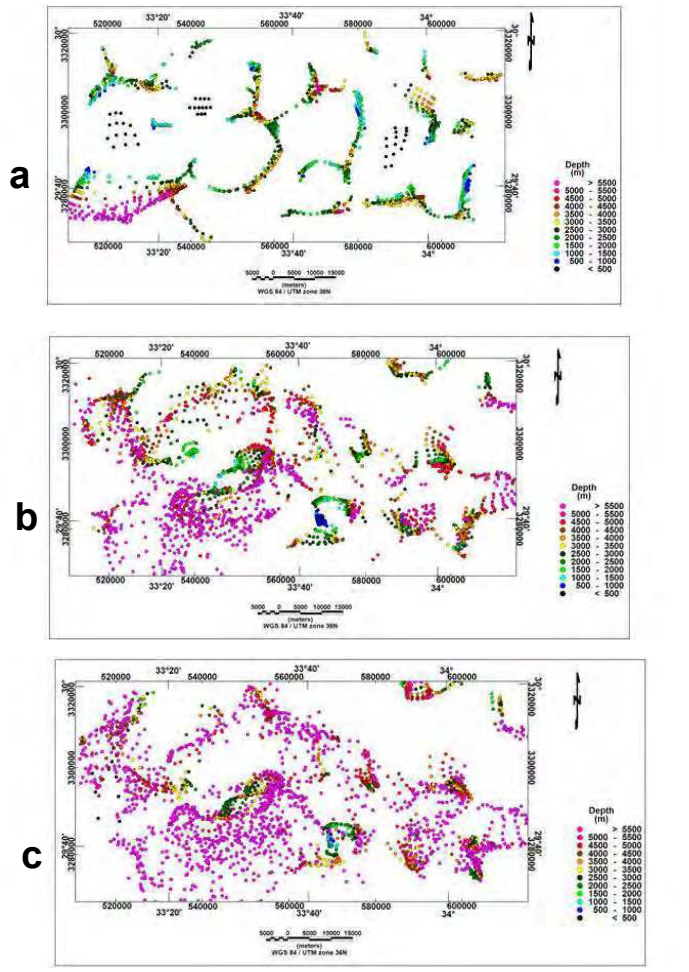

Fig.15: Euler deconvolution at a: SI=0, b: SI=1, c: SI=2

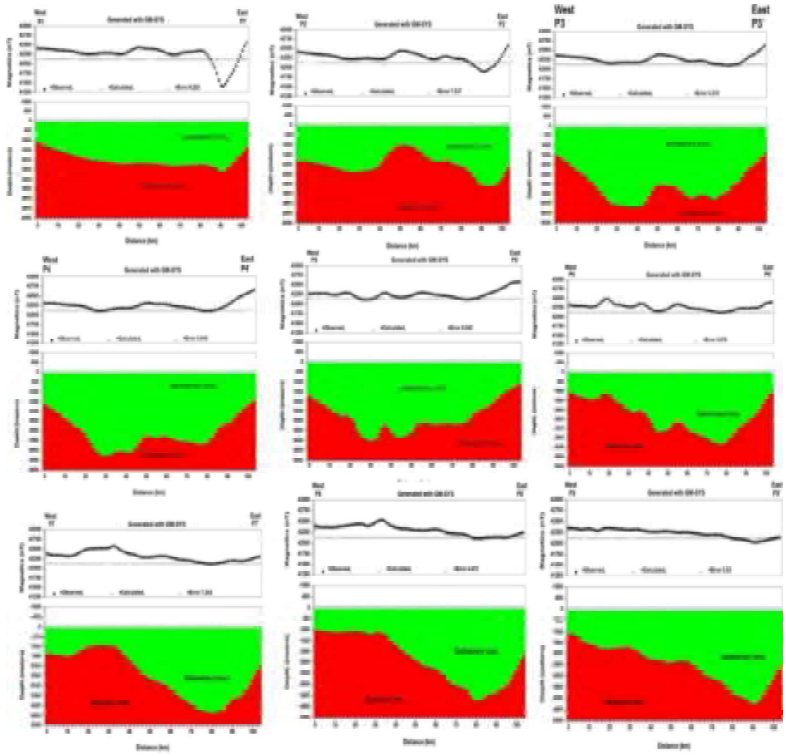

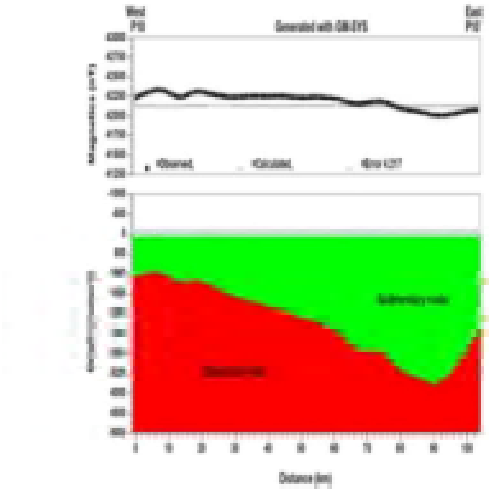

Fig. 16: Magnetic Models Along Profiles from P1-P1`to P10-P10`

The fourth order residual gravity anomaly map was used to detect the locations and trends of the fault elements dissecting the study area (Fig.14a), which indicated that the study area was dissected by different fault elements of different trends such as NE-SW and nearly N-S (Fig.14b).

The Euler deconvolution technique was applied on gravity anomaly map to determine the depth and trend of the structural elements dissecting the study area. The Euler deconvolution process was applied for different structural indices to define the best solution of the structural index where the best solution was represented by the solutions were coincidence and arranged in trends. The structural index (SI) is a measure of the fall-off rate of the field with distance from the source Oasis Montaj (2007). The following Table (3) showed an appropriate model for the structural index value. In the present study, the structural indices applied were 0, 1 and 2 (Fig15) to select the best solution of the structural index, where the SI = 0 seems the best solution as in Fig (15a), where the SI=0 refers to sill, dyke, Ribbon and step structure in the study area. Also, the trends of faults at SI=0 were nearly similar to the fault elements, which were detected from the least squares residual map.

Table 3: Structure Index (SI) at Gravity Field

SI	Gravity field
0	Sill/Dyke/Rippon/Step
1	Cylinder/Pipe
2	sphere
3	N/A

The main target of the magnetic data is to determine the depth to the top of the basement surface, that produces the observed anomalies. The quantitative interpretation of the magnetic data map was carried out through 2-D magnetic modeling by using GM-SYS software (Oasis Montag, 2007). In this work, ten profiles trending W–E were modeled (Fig.16). The magnetic susceptibility of the basement was assumed to be constant with a value of 0.00535 CGS unit (0.0672 SI unit). This parameter was used in the modeling of the ten profiles. The models in Fig (16) showed the variations in the thickness of the sedimentary sequence and of the topography of the top of the basement rocks. These results were used to draw the map of the basement surface depth. The depth of basement surface (Fig.17) indicated that, the basement depth ranged between 1005 m and 4108m in the study area. The basement depths found in the middle and north of the study area were very deep, which had values more than 2800 m, but to the east, south and west of the study area were of shallow depths, where the depth had values less than 1000 m. So the general dip of basement in the study area (from shallow to deep) directs from the east, south and west toward northeast.

The results of geoelectric data are conformed with the results of borehole (Jica1) for the lithology and depth of aquifer and the water quality where the TDS of water samples from boreholes was 1206 ppm which is more or less fresh water where the aquifer reflects relatively high resistivity value ranging from 26.5-477 Ohm.m. The fault elements which were delineated from gravity interpretation are indicated on the geological map of the study area.

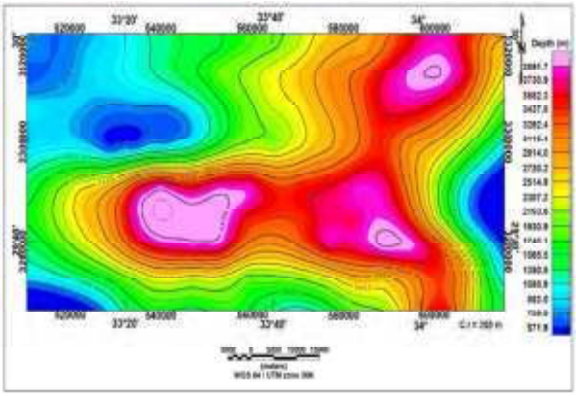

Fig. 17: Basement Relief Map of the Study Area

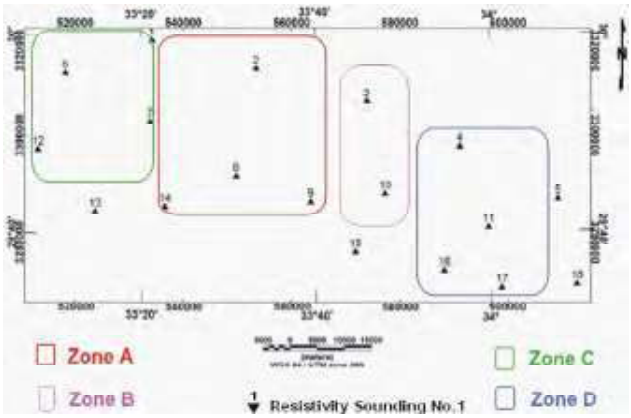

Fig. 18: Location of Geoelectric VES Stations with the Priority Zones to Detect the Best Places for Drilling Plan in the Study Area

CONCLUSION

From the results of the integrated geophysical interpretation of the study area, we can conclude that the study area contains deep groundwater aquifer (Nubian Sandstone aquifer) at depths ranging from718 m to 927 m and thicknesses ranging from 191 m to 3330 m and the resistivity values ranging from 26.5 Ohm m to 477 Ohm m. The result of interpretation of the gravity data indicated that, the main structural elements are well correlated with the Gulf of Aquba (NW–SE) and the Nile Valley (N–S) trends. From the 2-D magnetic modeling, the depth of the basement rocks was ranging from 1005 m to 4108 m in the study area.

Recommendation: According to the integrated geophysical interpretation, we can give recommendation about the best sets for drilling plan. The study area can be divided into three zones, according to the less depth, greater thickness and high resistivity, for the groundwater aquifer and the quality of water for the aquifer. According to the results of the geophysical interpretation, the best zone for drilling plan in the study area is the zone A Fig (18).

REFERENCES

1. Goldman M. and F.M. Neubauer, 2004. Groundwater Exploration Using Integrated Geophysical Techniques", Surveys in Geophysics, 15(3): 331-361.
2. Kearey, P. and M. Brook, 2002. An Introduction to Geophysical Exploration, 4th edition. Blackwell Science, pp: 254.
3. Murty, B.V.S. and V.K. Raghavan, 2002. The Gravity Method in Groundwater Exploration in Crystalline Rocks: a Study in the Peninsular Granitic Region of Hyderabad, India", Hydrogeology Journal, 10(2002), pp: 307-321.DOI.10.1007/s10040-001-0184-2.
4. UNESCO, 2005: Geologic Map of Sinai, Egypt, Scale 1: 500,000, Project for the Capacity Building of the Egyptian Geological survey and Mining Authority and the National Authority for Remote Sensing and Space Science in Cooperation with UNDP and UNSECO., Geological Survey of Egypt.
5. Geological Description of the Borehole JICA 1 Well: (after JICA, 1992, EGSMA, 1996 and Ghobachi, 2010).
6. Ward, S.H., 1990. Geotechnical and Environmental Geophysics Series Investigations in Geophysics, vol. 5. Society of Exploration Geophysics, Tulsa, USA.
7. Sultan, S.A., F.A. Santos and A. Helal, 2006. A study of the Groundwater Seepage on Hibis Temple Using Geoelectrical Data, Kharaga, Egypt, Egypt, near surface geophysics Journal, pp: 347-354.
8. Araffa, S.A.S., 2010. Geophysical investigation for shallow subsurface geotechnical problems of Mokattam area, Cairo, Egypt, Environmental Earth Sciences Journal, 59: 1195-2207.

9. Araffa, S.A.S., H.M. El Shayeb, M.F. AbuHashesh and N.M. Hassan, 2015: Delineating subsurface structure and assessment of groundwater aquifer using integrated geophysical interpretation at the central part of Sinai, Egypt, journal of Geoscience, First online, pp: 305-318.DoI: 10.1007/s12517-015-1824-5.
10. Koefoed, O., 1960: A generalized Cagniard graph for interpretation of geoelectrical sounding data. Geophysical prospecting, 8(3): 459-469.
11. Orellana, E. and H.M. Mooney, 1966. Master table and curves for vertical electrical sounding data, Geophysical Prospecting, 8(3): 459-469.
12. Chuansheng, W., Jinrong and Z. Xiufen, 2008. AGenetic Algorithm Approach for Selecting Tikhonov Regularization Parameter, IEEE Congress on Evolutionary Computation (CEC 2008).
13. Oasis Montaj, 2007. Geosoft mapping and application system, Inc., Suit 500, Richmond St. West Toronto, ON, Canada N5SIV6.
14. Baranov, V., 1957. A New Method for Interpretation of Aeromagnetic Maps: Pseudo- Gravimetric Anomalies, Geophysics, 22: 359-383.
15. Baranov, V. and H. Naudy, 1964. Numerical Calculation of the Formula of Reduction to the Magnetic Pole, Geophysics, 29: 67-79.
16. Bhattacharyya, B.K., 1965. Two dimensional harmonic analysis as a tool for magnetic interpretation; Geophysics, 30(5): 829-857.
17. Baranov, V., 1975. Potential Fields and Their Transformation in Applied Geophysics, Geoexploration Monographs, Series1-6. Berlin – Stuttgart: Gebrüder, Borntraeger.